Int. J. Electrochem. Sci., 16 **(2021)** Article ID: 210631, doi: 10.20964/2021.06.41

International Journal of
ELECTROCHEMICAL
SCIENCE
www.electrochemsci.org

Synthesis of Hollow Paramontroseite VO_2 Microspheres as Stable Electrode Materials for Lithium-ion Batteries

Hailong Fei

State Key Laboratory of Photocatalysis on Energy and Environment, College of Chemistry, Fuzhou University, Fuzhou, Fujian 350002, China
E-mail: hailongfei@fzu.edu.cn

Received: 18 February 2021 / *Accepted:* 4 April 2021 / *Published:* 30 April 2021

A simple and versatile method was developed to prepare hollow Paramontroseite VO_2 microspheres. Hollow VO_2 microspheres were formed via an Ostwald ripening mechanism. The morphology, crystalline structure and electrochemical performance were systematically studied. It was found that hollow Paramontroseite VO_2 microspheres can be used as stable anode and cathode materials for lithium-ion batteries with acceptable rate cycling performance. In addition, the discharge capacities of hollow paramontroseite VO_2 microsphere-based negative electrodes were found to reach 384.2 $mAhg^{-1}$ at a current density of 750 mAg^{-1}. A discharge capacity of 195.6 mAg^{-1} was achieved when the microspheres were used as a cathode material for lithium-ion batteries at a current density of 20 mAg^{-1}. Vanadium-based dual electrode materials are seldom reported in the literature.

Keywords: Paramontroseite VO_2; Hollow microspheres; Anode; Lithium-ion battery; Cathode

1. INTRODUCTION

Vanadium-containing micro/nanostructures have attracted much interest owing to their excellent properties related to lithium-ion batteries [1, 2], sodium-ion batteries [3], potassium-ion batteries [4], zinc-ion batteries [5] and catalysis [6, 7], which are of significant importance to fundamental science, technology and energy [8]. Among various vanadium oxides, vanadates and ammonium vanadium bronzes, VO_2 is well known and the most promising for low electronic thermal conductivity [9] and ultrafast solid phase transitions [10] in the opinion of physicists. Paramontroseite VO_2 has received little attention because it has been difficult to prepare at a large scale in the past decade. Paramontroseite VO_2 can be prepared via hydrothermal carbonization of sucrose in the presence of ammonium metavanadate and oxalic acid [11]. Under hydrothermal conditions, thioacetamide (TAA) can reduce sodium orthovanadate ($Na3VO_4 \cdot 12H_2O$) to paramontroseite VO_2 [12]. In addition, montroseite VOOH can be converted to paramontroseite VO_2 after annealing [13, 14]. In the presence of GeO_2, citric acid

monohydrate ($C_6H_8O_7 \cdot H_2O$) can also reduce V_2O_5 to Ge^{4+}-modified paramontroseite VO_2 after hydrothermal treatment [15]. Paramontroseite VO_2 has some potential applications in batteries and therapeutics [16]. VO_2(p) nanorods can synergize with V_2C to enhance the adsorption capacity of the host for lithium polysulfides and reduce the redox reaction barrier in the conversion of polysulfides to short-chain sulfides, which leads Li-S batteries to exhibit outstanding electrochemical performance and excellent reversible discharge capacity (1250 $mAh \cdot g^{-1}$ at 0.2 C) and long-term cycling stability [17]. The VO_2 (P)-NCNT/S cathode exhibits excellent performance because VO_2 (P) nanoparticles function as catalysts to oxidize LiPS to produce thiosulfate due to strong chemical interactions [18]. In addition, thiosulfates act as mediators to catenate long-chain LiPS together and convert short-chain Li_2S_2/Li_2S and surface-bound polythionate complexes [18]. The paramontroseite $VO_2/LiMn_2O_4$ cell exhibits a discharge capacity of 45.96 mAh g^{-1} after 50 cycles at a current density of 60 mA g^{-1} between 0.5 and 1.7 V in aqueous electrolyte [12]. As a cathode material for lithium-ion batteries, paramontroseite VO_2 nanoparticle carbonaceous core-shell microspheres have a discharge capacity of 133.2 mA g^{-1} between 1.0 and 3.4 V in non-aqueous electrolyte [11]. The discharge capacity and cycling stability of paramontroseite VO_2 for lithium-ion batteries still need to be improved dramatically.

It has been reported that hollow and sphere-like electrode materials have shown good electrochemical performance for batteries due to their benefits, including their enhancement of electron pathways, effective accommodation of volume changes, anti-pulverization ability, electrochemical kinetics, tap density, high specific surface area, large load capacity and low density, electron transfer impedance and ion transfer[19-36]. Herein, we develop a simple and versatile method for the preparation of hollow nanoparticle-accumulated paramontroseite VO_2 microspheres via in situ sacrifice of $Mn_4V_2O_9$ core/shell microspheres. First, both hollow paramontroseite VO_2 microspheres and $Mn_4V_2O_9$ core/shell microspheres were used as anode materials for lithium-ion batteries. The former showed higher discharge capacity and better rate performance than the latter. In addition, it was found that hollow paramontroseite VO_2 microspheres can be used as cathode materials for lithium-ion batteries with a higher discharge capacity than the reported 133.2 mA g^{-1} in the literature.

2. EXPERIMENTAL

In a typical procedure, the 30 ml mixed aqueous solution of 1 mmol ammonium vanadate and 1 mmol manganese acetate tetrahydrate was transferred into a 50-ml Teflon-lined stainless autoclave and maintained at 120-250 °C for various times. The temperature in the autoclave was dropped to room temperature. A dry black-green powder formed after filtering, washing with deionized water, and drying at 110 °C for 3 h.

A Hitachi S-4800 field emission scanning electron microscope (FE-SEM) was used to investigate the surface morphology of the samples. X-ray diffraction (XRD) patterns were recorded on a diffractometer (Co Kα, PANalytical, XPert, data were converted into Cu Kα) from 5 to 70 degrees. A Land CT 2001A cycle life tester was used to record the charge-discharge cycles. The CV tests were performed with a CHI660 electrochemical workstation from 0.05 to 3.0 V at a scan rate of 1 mV/S. The

impedance data was obtained with a Zahner IM6 electrochemical workstation from 5 MHz to 0.1 Hz frequency at a 5 mV acoscillation amplitude.

The synthesized hollow paramontroseite VO_2 microspheres can be used as anode and cathode materials for lithium-ion batteries. The negative and positive electrodes were prepared by pasting a slurry of the active material, acetylene black, and polyvinylidene fluoride with a weight ratio of 6:3:1 onto circular Cu and Al foil flakes, respectively. The flakes were dried at 110 °C for 3 h under vacuum. The metallic lithium foil was used as the counter electrode. The electrolyte was 1 M $LiPF_6$ in a mixed solvent of ethylene carbonate, dimethyl carbonate and diethylene carbonate with a volume ratio of 1:1:1. All of the CR2025 cells were assembled in an argon-filled glove box. The assemble and tests of paramontroseite VO_2 microspheres at 1 and 3.5 h based anode were also tested under the identical conditions.

3. RESULTS AND DISCUSSION

The X-ray diffraction (XRD) patterns of the samples are shown in Figure 1. The reaction time had a dramatic effect on the crystalline structure of products. After 1 h of reaction time, the diffraction pattern showed the crystalline precursor, $Mn_4V_2O_9$ (JCPDS 31-0849), as shown in Figure 1a. As the reaction time increased to 2 and 3.5 h, the obtained $Mn_4V_2O_9$ exhibited weaker diffraction peaks of (-603) and (201) in Figures 1b and 1c, respectively. Paramontroseite VO_2 (JCPDS 25-1003) was reached when the reaction time was prolonged to 24 h, as confirmed in Figure 1d. The $Mn_4V_2O_9$ phase disappeared from the XRD pattern of paramontroseite VO_2.

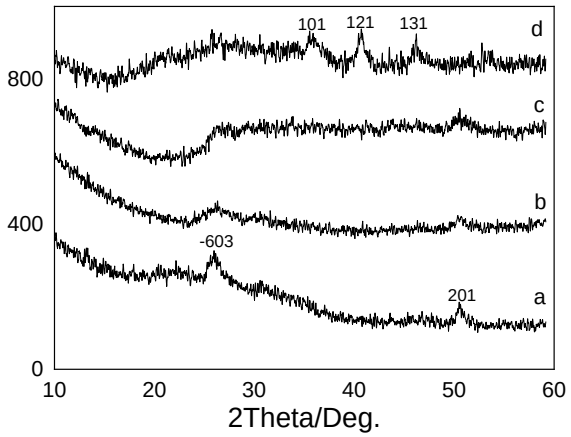

Figure 1. XRD patterns of the samples prepared at different reaction times: (a) 1 h, (b) 2 h, (c) 3.5 h and (d) 24 h.

The surface morphology information of the sample prepared at different reaction times is shown in Figure 2. The sample obtained at 1 h had sphere-like particles, shown in Figure 2a. The magnified SEM image shows that some microspheres had a core-shell structure. The core was solid, while the shell was made up of nanoparticles, as shown in Figure 2b. Both the number and size of core-shell microspheres increased in the samples obtained after 2 and 3.5 h of reaction time, as shown in Figures

2c and 2e. Figures 2d and 2f show that the core was also made up of nanoparticles. When the hydrothermal treatment time was 24 h, hollow microspheres formed, as shown in Figure 2e. The diameters of the microspheres were in the range of several micrometres. The microspheres had a nanoparticle-like surface.

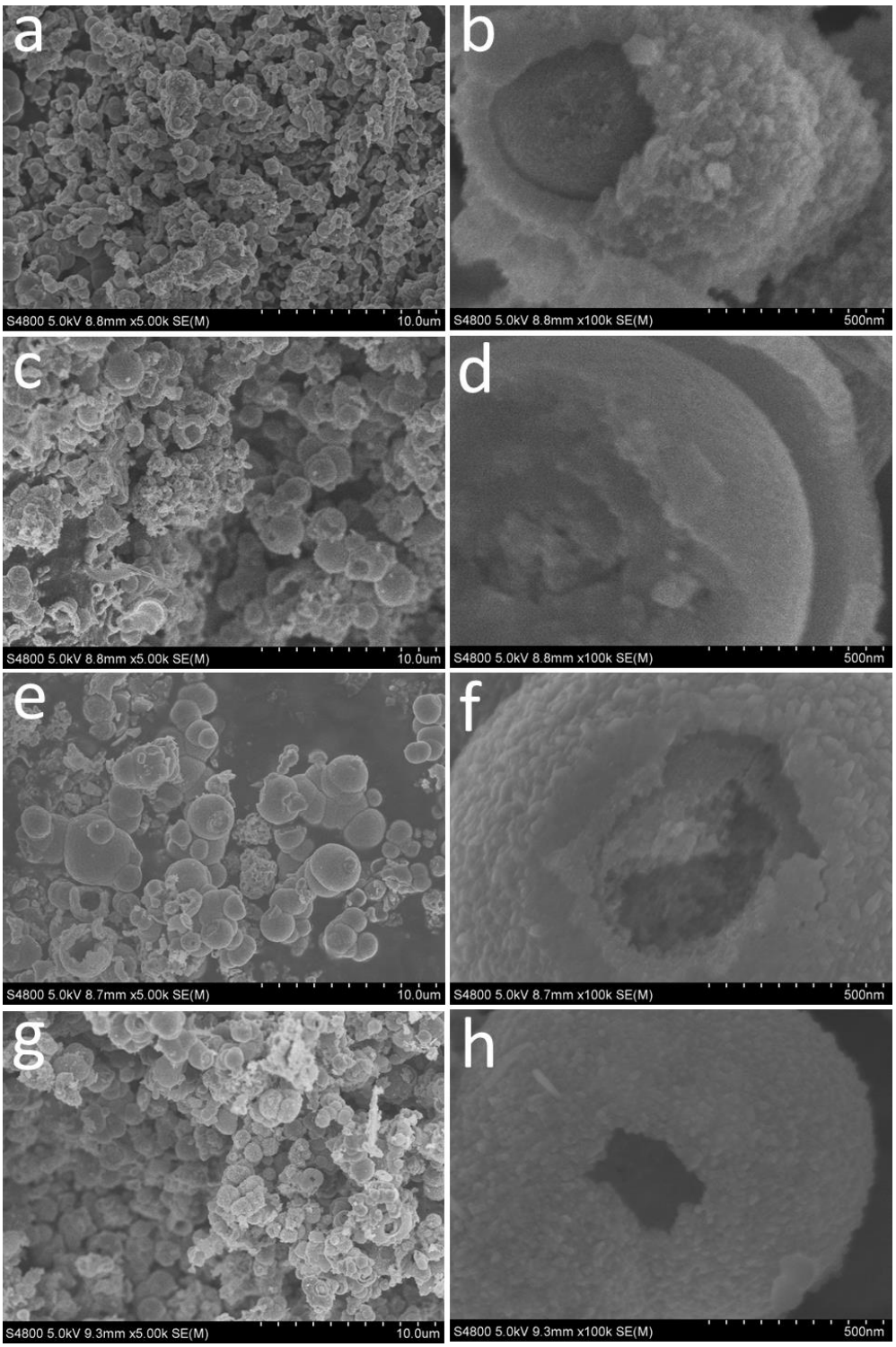

Figure 2. SEM images of the samples prepared at different reaction times: (a, b) 1 h, (c, d) 2 h, (e, f) 3.5 h and (g, h) 24 h.

Based on the above experimental results, we proposed that hollow paramontroseite VO_2 microspheres formed via Ostwald ripening. In the initial stage of the reaction, primary $Mn_4V_2O_9$ and VOx crystallites organized into microspheres with smaller surface energy and a crystallite-size distribution in which large crystallites were located on the outermost surface. The large crystallites on the outermost surface grew at the expense of small crystallites inside via Ostwald ripening to form core/shell microspheres [37]. With increasing reaction time, metastable $Mn_4V_2O_9$ converted to stable paramontroseite VO_2, so hollow paramontroseite VO_2 microspheres finally formed by consuming $Mn_4V_2O_9$.

Figure 3 shows the cyclic voltammetry (CV) curves of hollow paramontroseite VO_2 microspheres (24 h) and $Mn_4V_2O_9$ core/shell microspheres (1 h). The voltammograms of the $Mn_4V_2O_9$ core/shell microspheres show two pairs of peaks, (0.77 V, 1.1 V) and (1.68 V, 2.37 V), in Figure 3a. The first CV cycle of hollow paramontroseite VO_2 microspheres exhibited small cathodic peaks at 0.63 and 1.69 V. In the second cycle, the peak at 0.63 V disappeared due to the formation of SEI film. The peak at 1.69 V shifted to 1.92 V. During later cycles, the pair of peaks (1.92 V, 2.34 V) never moved.

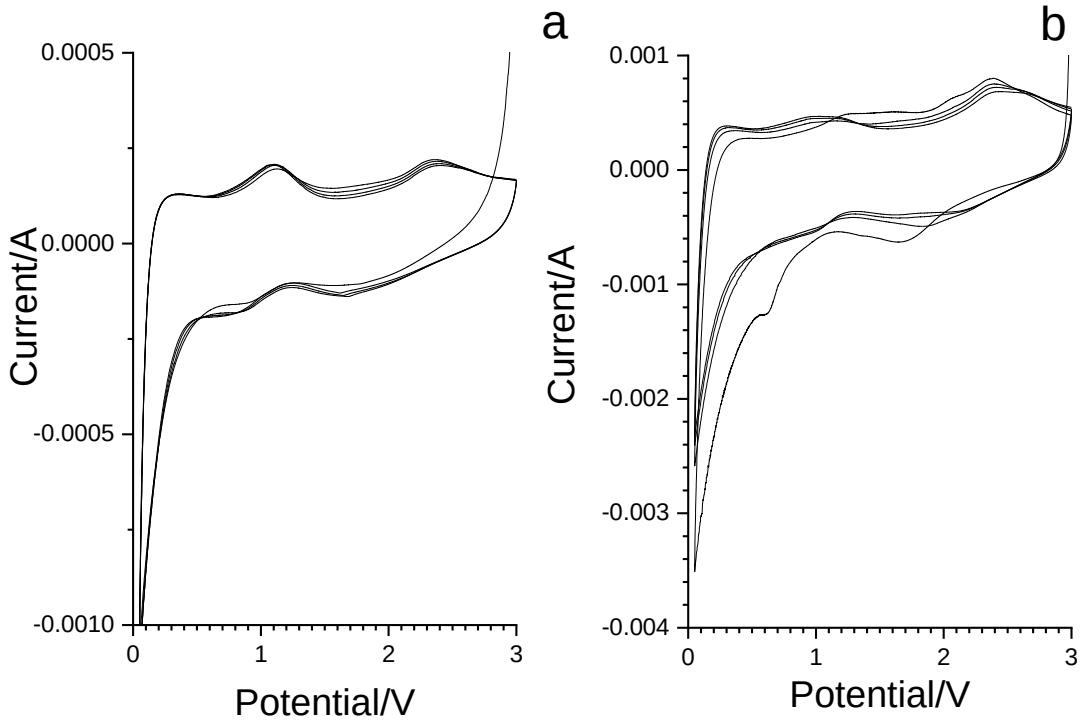

Figure 3. Cyclic voltammograms of samples prepared at different reaction times at a scan rate of 1 mV/s: (a) 1 h and (b) 24 h.

The 2nd and 250th discharge profiles of hollow paramontroseite VO_2 microspheres at a discharge current of 750 mAg^{-1} are shown in Figure 4a. The two curves have similar shapes, which implies good cycling performance. The discharge capacities were 384.2 and 338.1 $mAhg^{-1}$, respectively. The hollow paramontroseite VO_2 microspheres showed a higher discharge capacity than the $Mn_4V_2O_9$ core/shell microspheres prepared for 1 and 3.5 h, as shown in Figure 4b. The electrode of the hollow paramontroseite VO_2 microspheres could perform 250 cycles. However, the $Mn_4V_2O_9$ core/shell

microspheres showed both a very low discharge capacity and poor cycling stability. The corresponding discharge rate capability of hollow Paramontroseite VO_2 microspheres was tested at current densities of 100, 250, 500, 750, 1000, 1250, 1500 and 100 mAg^{-1} (Figure 4c) and exhibited a stable discharge capacity at various discharge rates, as shown in Figure 4c. The second discharge capacity was 575.4 $mAhg^{-1}$, while the 90th discharge capacity was 499.2 $mAhg^{-1}$. The capacity retention was as high as 86.8% after 90 cycles. Although the $Mn_4V_2O_9$ core/shell microspheres also showed good rate cycling performance at current densities of 100, 250, 500, 750, 1000, 1250 and 100 mAg^{-1}, the second discharge capacity was low at 377.6 $mAhg^{-1}$, while the 85th discharge capacity was 245.5 $mAhg^{-1}$. The capacity retention was 65% after 85 cycles.

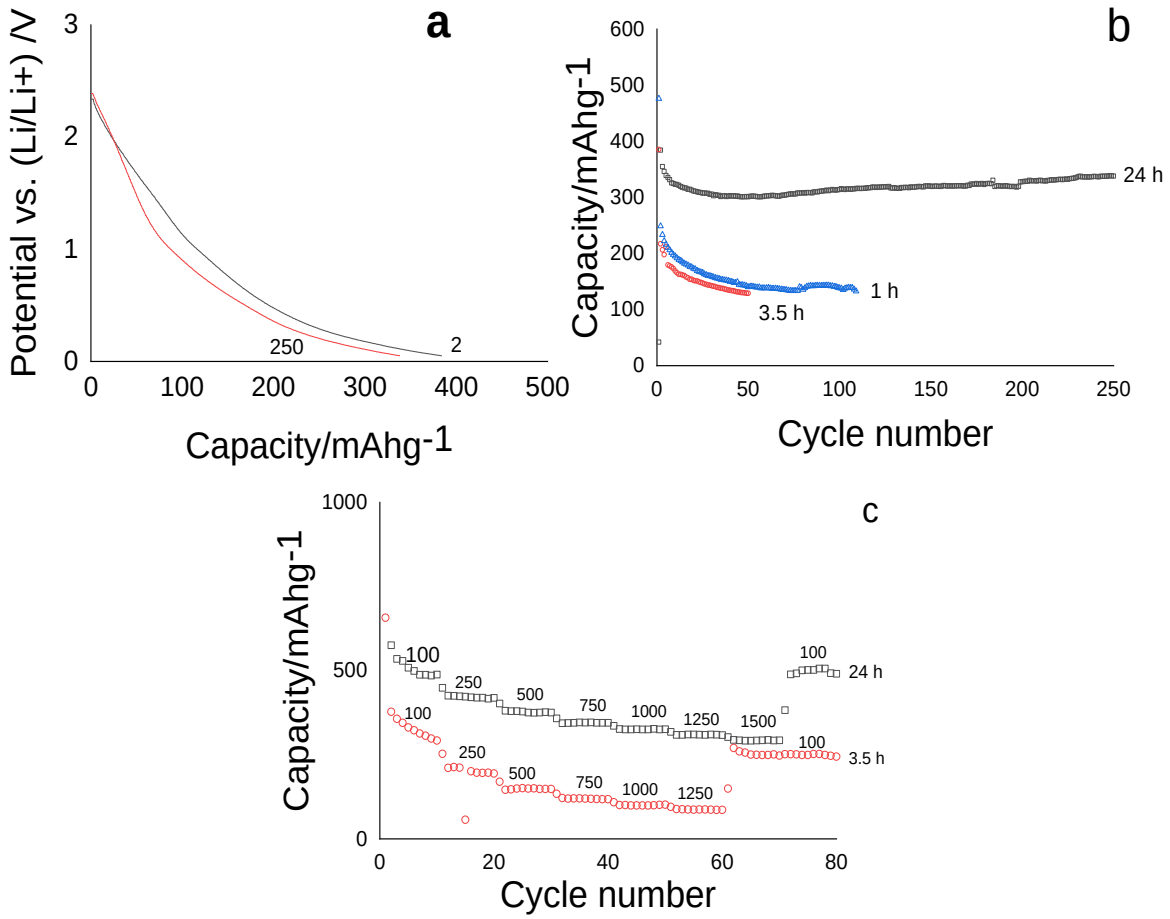

Figure 4. The discharge curves of paramontroseite VO_2 microspheres at a current density of 750 mAg^{-1} between 0.05 and 3.0 V (a), the cycle performance of samples prepared at different times (1, 3.5 and 24 h) (b), and the evolution of the reversible capacity for samples prepared at 3.5 and 24 h at various current densities (c).

Hollow paramontroseite VO_2 microspheres can also be good cathode materials for lithium-ion batteries. Figure 5a shows the 2nd and 50th discharge profiles of hollow paramontroseite VO_2 microspheres at discharge currents of 20 mAg^{-1} with discharge capacities of 195 and 156 $mAhg^{-1}$,

respectively. The capacity shown is much higher than that of paramontroseite VO_2 carbonaceous core-shell microspheres (133.2 mAhg-1) [11]. After cycling, the slope of the 50th discharge curve plateaued between 2.9 and 3 V, which implies slow capacity decay in this range. Figure 5b shows the corresponding cycling performance at a discharge current of 20 mAg^{-1}. The electrode of the hollow Paramontroseite VO_2 microspheres cycled 50 times with a capacity retention of 80%. The corresponding discharge rate capability of the hollow paramontroseite VO_2 microspheres was also tested at current densities of 20, 40, 100, 200, 300, 400 and 20 mAg^{-1} (Figure 4c) and exhibited a stable discharge capacity, as shown in Figure 5c. The capacity retention was 60% after 77 cycles.

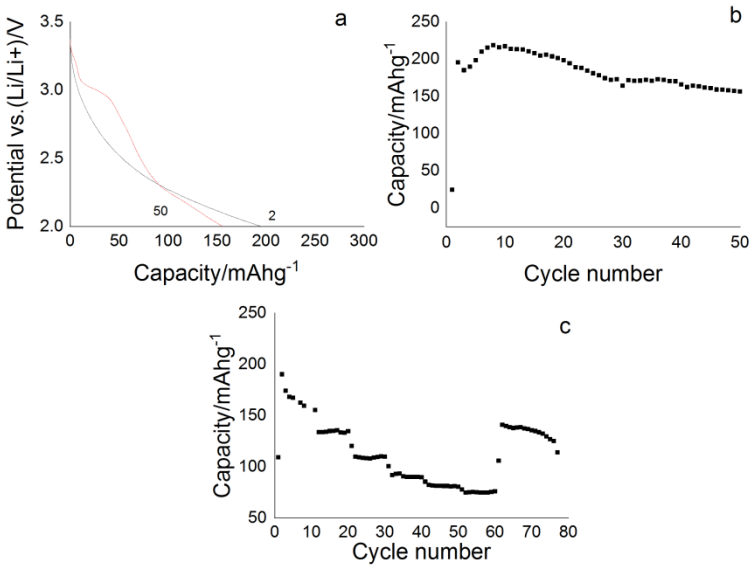

Figure 5. The 2nd and 50th discharge curves of paramontroseite VO_2 microspheres at a current density of 20 mAg^{-1} between 2.0 and 3.4 V (a), the cycle performance at a current density of 20 mAg^{-1} (b), and the evolution of the reversible capacity at various current densities (c).

Electrochemical impedance measurements elucidate the difference in electrochemical properties of hollow paramontroseite VO_2 microsphere and $Mn_4V_2O_9$ core/shell microsphere electrodes, as shown in Figure 5. The fitted equivalent electrical circuit model is at the top of Figure 5. R_S is the active electrolyte resistance. C1 and C2 are the double-layer capacitance. The impedance of a faradaic reaction is made up of an active charge transfer resistance Rct and a specific electrochemical element of diffusion W, the Warburg element. Rf is the fixed impedance of the cell. The fitted values of Rs, Rct, Rf, W, C1 and C2 are 5.69, 120.38, 100.58, 3.07 x 10^{-3}, 7.74 x 10^{-5} and 3.29 x 10^{-6} Ω for the hollow paramontroseite VO_2 microspheres and 6.51, 51.57, 151.32, 2.58 x 10^{-3}, 1.76 x 10^{-4} and 2.86 x 10^{-6} Ω for the $Mn_4V_2O_9$ core/shell microspheres, respectively. $Mn_4V_2O_9$ core/shell microspheres have smaller charge transfer resistance than hollow paramontroseite VO_2 microspheres. However, paramontroseite VO_2 is more stable than $Mn_4V_2O_9$ core/shell microspheres during the process of inserting/de-inserting lithium ions. This is the reason that hollow paramontroseite VO_2 microspheres have better electrochemical properties than those of $Mn_4V_2O_9$ core/shell microspheres.

Electrochemical impedance measurements elucidate the difference in electrochemical properties of hollow paramontroseite VO_2 microsphere and $Mn_4V_2O_9$ core/shell microsphere electrodes, as shown in Figure 5. The fitted equivalent electrical circuit model is at the top of Figure 5. R_S is the active electrolyte resistance. C1 and C2 are the double-layer capacitance. The impedance of a faradaic reaction is made up of an active charge transfer resistance Rct and a specific electrochemical element of diffusion W, the Warburg element. Rf is the fixed impedance of the cell. The fitted values of Rs, Rct, Rf, W, C1 and C2 are 5.69, 120.38, 100.58, 3.07 x 10^{-3}, 7.74 x 10^{-5} and 3.29 x 10^{-6} Ω for the hollow paramontroseite VO_2 microspheres and 6.51, 51.57, 151.32, 2.58 x 10^{-3}, 1.76 x 10^{-4} and 2.86 x 10^{-6} Ω for the $Mn_4V_2O_9$ core/shell microspheres, respectively. $Mn_4V_2O_9$ core/shell microspheres have smaller charge transfer resistance than hollow paramontroseite VO_2 microspheres. However, paramontroseite VO_2 is more stable than $Mn_4V_2O_9$ core/shell microspheres during the process of inserting/de-inserting lithium ions. This is the reason that hollow paramontroseite VO_2 microspheres have better electrochemical properties than those of $Mn_4V_2O_9$ core/shell microspheres.

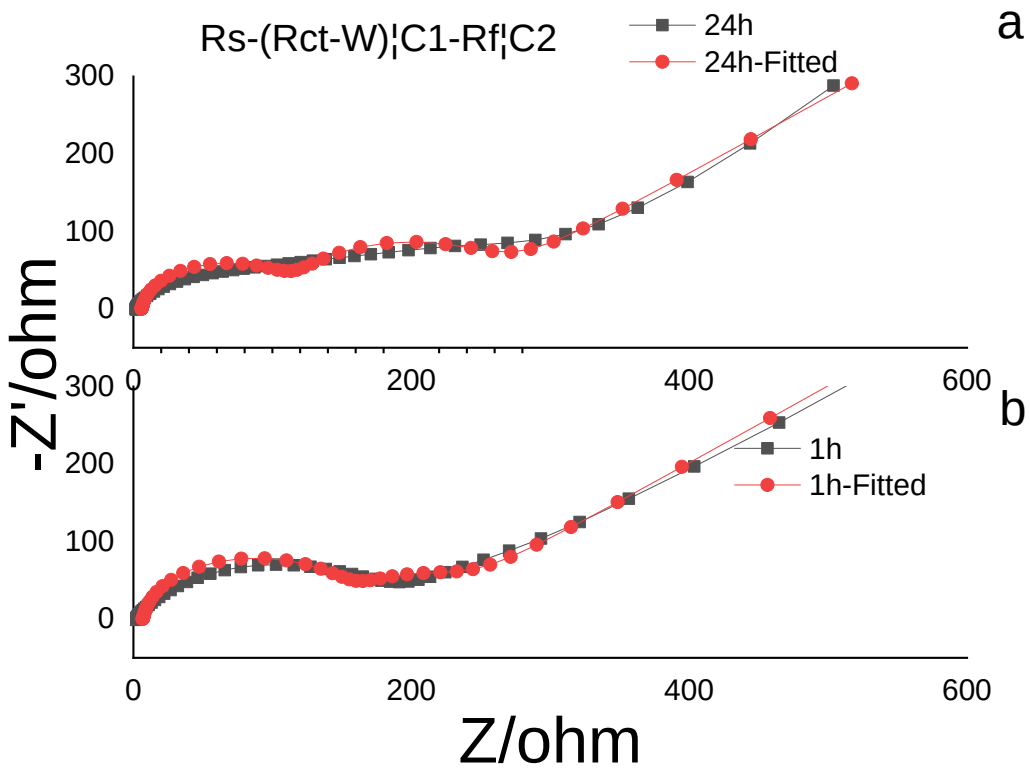

Figure 6. Fitted and unfitted Nyquist diagrams of samples prepared at different reaction times: (a) 24 h and (b) 1 h (the top is the fitted impedance circuit model).

4. CONCLUSIONS

In summary, $Mn_4V_2O_9$ core/shell microspheres were prepared via Ostwald ripening and were further converted to stable hollow paramontroseite VO_2 microspheres after long hydrothermal treatment. Both types of microspheres can be stable anode materials for lithium-ion batteries. The hollow paramontroseite VO_2 microspheres showed a higher discharge capacity and better cycling stability

ascribed to novel morphologies compared to their counterparts. In addition, hollow paramontroseite VO_2 microspheres also had a higher discharge capacity as a cathode material for lithium-ion batteries; this property could shed some light on dual electrode materials for batteries.

ACKNOWLEDGEMENTS
The project was supported by National Science Foundation of China (Grants No. 51204058).

References

1. H.D. Liu, Z.Y. Liu, Q.Z. Zhu, Q.Z. Yan, S.C. Yu, X. He, Y. Chen, R. Zhang, L. Ma, T.C. Liu, M. Li, R.Q. Lin, Y.M. Chen, Y.J. Li, X. Xing, Y. Choi, L. Gao, H.S.Y. Cho, K. An, J. Feng, R. Kostecki, K. Amine, T.P. Wu, J. Lu, H.L.L. Xin, S.P. Ong, P, Liu, *Nature*, 585 (2020) 63.
2. F.Y. Cheng, J. Chen, *J. Mater. Chem.,* 21(2011) 9841-9848.
3. Q.H. Wang, J.T. Xu, W.C. Zhang, M.L. Mao, Z.X. Wei, L. Wang, C.Y. Cui, Y.X. Zhu, J.M. Mam, *J. Mater. Chem*., 6 (2018) 8815-8838.
4. M.Z. Chen, Q.N. Liu, Z. Hu, Y.Y. Zhang, G.C. Xing, Y. X. Tang, S. L. Chou, *Adv. Energy Mater*., 10 (2020) 2002244.
5. N. Zhang, M. Jia, Y. Dong, Y.Y. Wang, J.Z. Xu, Y.C. Liu, L.F. Jiao, F.Y. Cheng, *Adv. Func. Mater*., 29 (2018) 1807331.
6. B. Schwarz, J. Forster, M. K. Goetz, D. Yîcel, C. Berger,T. Jacob, C. Streb, *Angew. Chem. Int. Ed*., 55 (2016) 6329 –6333.
7. K. Fan, Y.F. Ji, H.Y. Zou, J.F. Zhang, B.C. Zhu, H. Chen, Q. Daniel, Y. Luo, J.G. Yu, L.C. Sun, *Angew. Chem. Int. Ed*. 56 (2017) 1 – 6.
8. Y. Wang, H.L. Fei, *Ionics*, 19 (2013) 771-776.
9. S. Lee, K. Hippalgaonkar, F. Yang, J.W. Hong, C. Ko, J. Suh, K. Liu, K. Wang, J. J. Urban, X. Zhang, *Science*, 355 (2017) 371.
10. S. Wall, S. Yang, L. Vidas, M. Chollet, J.M. Glownia, M. Kozina, T. Katayama, T. Henighan, M. Jiang, T.A. Miller, *Scienc*e, 362 (2018) 572.
11. H.L. Fei, X.K. Ding, M. Wei, K.M. Wei, *Solid State Sci*., 13 (2011) 2049-2054.
12. C.Z. Wu, Z.P. Hu, W. Wang, M. Zhang, J.L. Yang, Y. Xie, *Chem. Commun*., 33 (2008) 3891–3893.
13. Y. Xu, L. Zheng, Y. Xie, *Dalton Trans*., 39 (2010) 10729–10738.
14. C.Z. Wu, F. Feng, J. Feng, J. Dai, J.L. Yang, Y. Xie, *J. Phys. Chem. C* 115 (2011) 791–799.
15. M. Saini, R. Malik, S. Lata, B. Saini, P. Kumar, B.S. Dehiya, H.K. Seo, A. Umar, *J. Mater. Sci.-Mater. IN Electron*., 31 (2020) 3795-3802.
16. W. Zhou, Y.Y. n Miao, Y.J. Zhang, L. Liu, J. Lin, J. Y Yang, Y. Xie, L.P. Wen, *Nanotech.,* 24 (2013) 165102.
17. Z.G. Wang, K. Yu, Y. Feng, R.J. Qi, J. Ren, Z.Q. Zhang, *ACS Appl. Mater. Interfaces*, 11 (2019) 44282−44292.
18. S.Z. Wang, J.X. Liao, X.F. Yang, J.N. Liang, Q. Sun, J.W. Liang, F.P. Zhao, A. Koo, F.P. Kong, Y. Yao, X.J. Gao, M.Q. Wu, S.Z. Yangc, R.Y. Li, X.L. Sun, *Nano Eng.*, 57 (2019) 230–240.
19. Lim, SY, *Solid State Sci*., 96 (2019) 105949.
20. P.Tian, Q. Song, H.C. Pang, G.L. Ning, *Mater. Lett.*, 227 (2018) 13-16.
21. X. Liang, G.H. Gao, G.M.Wu, *Data In Briff*., 18 (2018) 719-722.
22. Y.P. Wang, Z.W. Nie, A.Q. Pan, Y.F. Zhang, X.Z. Kong, T. Zhu, S.Q. Liang, G.Z. Cao, *J. Mater. Chem. A*, 6 (2018) 6792-6799.
23. J. Xiang, X.Y. Yu, U Paik, *J. Power Source*, 329 (2016) 190-196.
24. G. H. An, D.Y. Lee, H. J. Ahn, *ACS Appl. Mater. & Interf*., 8 (2016) 19466-19474.

25. P.F. Zhang, L.Z. Zhao, Q.Y. An, Q. L. Wei, L. Zhou, X.J. Wei, J.Z. Sheng, L.Q. Mai, Small, 12 (2016) 1082-1090.
26. Z. Fu, J.W. Wu, G.H. Luo, X.C. Lv, X.H. Gao, L.J., *Chem*., 79 (2016) 805-810.
27. X.C. Du, G. Huang, L.M. Wang Limin, Synthesis of Vanadium Pentoxide Hollow Microspheres and Application as Cathode in Rechargeable Mg Batteries, *Chinese J. Appl. Chem*., 35 (2015) 1462-1464.
28. E. Armstrong, M. Osiak, H. Geaney, C. Glynn, C. O'Dwyer, *Cryst. Eng. Comm*., 16 (2014) 10804-10815.
29. A.M.Cao, J.S.Hu, H.P.Liang, L.J. Wan, *Angew. Chem. Int. Ed*., 44 (2005) 4391-4395.
30. Z. Wang, L. Zhou, X.W.D. Lou, *Adv. Mater.* , 24 (2012) 1903-1911.
31. H.L. Fei, Z.W. Li, W.J. Feng, X. Liu, *Dalton Trans*., 44 (2015) 146-150.
32. H.L. Fei, X. Liu, Z.W. Li, *Chem. Eng. J*., 281 (2015) 453-458.
33. H.L. Fei, W.J. Feng, Y.S. Lin, *Solid State Sci*., 55 (2016) 36-41.
34. H.L. Fei, Y.Q. Lin, T. Xu, *Ionics*, 23 (2017) 1949-1954.
35. H.L. Fei, I*nt. J. Electrochem. Sci*., 4 (2019) 11560-11570.
36. H. L. Fei, X. Liu, Z. W. Li, W. J. Feng, *Electrochim. Acta*, 174 (2015) 1088-1095.
37. H.L. Fei, H.J. Zhou, J.W. Wang, P. C. Sun, D.T. Ding, T.H. Chen, *Solid State Sc*i., 10 (2008) 1276-1284.